Zitierweise: *Angew. Chem. Int. Ed.* **2023,** *62,* e202217814
doi.org/10.1002/anie.202217814

Self-assembly

Two-Dimensional Supramolecular Polymerization of DNA Amphiphiles is Driven by Sequence-Dependent DNA-Chromophore Interactions

Muhammad Ghufran Rafique, Jacob M. Remington, Finley Clark, Haochen Bai, Violeta Toader, Dmytro F. Perepichka, Jianing Li, and Hanadi F. Sleiman**

Abstract: Two-dimensional (2D) assemblies of water-soluble block copolymers have been limited by a dearth of systematic studies that relate polymer structure to pathway mechanism and supramolecular morphology. Here, we employ sequence-defined triblock DNA amphiphiles for the supramolecular polymerization of free-standing DNA nanosheets in water. Our systematic modulation of amphiphile sequence shows the alkyl chain core forming a cell membrane-like structure and the distal π-stacking chromophore block folding back to interact with the hydrophilic DNA block on the nanosheet surface. This interaction is crucial to sheet formation, marked by a chiral "signature", and sensitive to DNA sequence, where nanosheets form with a mixed sequence, but not with a homogeneous poly(thymine) sequence. This work opens the possibility of forming well-ordered, bilayer-like assemblies using a single DNA amphiphile for applications in cell sensing, nucleic acid therapeutic delivery and enzyme arrays.

Introduction

The arrangement of molecular building blocks into higher-order assemblies is a critical aspect of supramolecular polymerization mechanisms observed in natural systems.[1] Biological assemblies such as the two-dimensional (2D) lipid bilayers in cellular membranes[2] have inspired a diverse library of synthetic macromolecular motifs—ranging from conventionally synthesized homo- and block-copolymers[3] to bola- and sequence-defined amphiphiles—for the assembly of 2D morphologies at the nano-, meso- and microscales. The self-assembly of block copolymers (BCPs), in particular, leading to morphologically well-defined 2D nanostructures with narrow size distributions has been successfully achieved in organic or mixed media through crystallization-driven processes.[4–11] Efforts have also been made to extend this approach to purely aqueous systems using either dialysis techniques with conventional BCPs[12–15] or by directly employing sequence-defined peptides[16] or peptoids—synthetic, N-substituted glycine oligomers[17]—leading to peptide-mimetic, 2D structures in water.[18–25] However, the question of how the polymer sequence influences the assembly of these molecules requires systematic studies to elucidate general guidelines for controlled self-assembly.[26]

Within the context of block copolymer self-assembly, DNA amphiphiles have emerged as promising water-soluble building blocks for the construction of nanostructures of promising biological relevance.[27–29] These polymers comprise a single-stranded DNA (ssDNA) as the hydrophilic block linked covalently to a hydrophobic small-molecule, oligomer, or dendritic structure.[30] They can combine the programmability and predictability of Watson–Crick-Franklin interactions of DNA with the orthogonal interactions and long-range order of the hydrophobic block. The self-assembly of DNA amphiphiles in aqueous solution has yielded morphologically well-defined nanostructures such as spherical micelles[31–37] and vesicles (0D),[38–42] nanofibers[43–46] and nanoribbons[47–50] (1D) exhibiting surface addressability and multivalency with a dense corona of ssDNA. These nanostructures exhibit improved cellular internalization,[51] nuclease resistance,[52] biodistribution profiles,[53] gene silencing activity,[54] multivalent binding via aptamers,[55] and can serve as templates for DNA displacement reactions such as HCR[56] and as nanoreactors for DNA/RNA amphiphile synthesis.[57,58]

The self-assembly of free-standing nanosheets provides the opportunity to study how bioactive components arranged in 2D influence cellular interactions, leading to applications such as drug delivery,[59] cell sensing and stimulation,[60] and antimicrobial activity.[61] A DNA amphi-

[*] M. Ghufran Rafique, H. Bai, Dr. V. Toader, Prof. D. F. Perepichka, Prof. H. F. Sleiman
Department of Chemistry, McGill University
801 Sherbrooke St W, H3A0B8 Montréal, QC (Canada)
E-mail: hanadi.sleiman@mcgill.ca
Dr. J. M. Remington, F. Clark, Prof. J. Li
Department of Chemistry, The University of Vermont
05405 Burlington, VT (USA)
Prof. J. Li
Current address: Department of Medicinal Chemistry and Molecular Pharmacology, Purdue University
West Lafayette, IN 47907 (USA)
E-mail: jianing-li@purdue.edu

phile-based system would expand these applications further into areas such as delivery of oligonucleotide therapeutics, DNA-binding protein capture and DNA-zyme cascades, owing to the sheets' high surface-to-volume ratios. However, only a handful of DNA amphiphile-based 2D structures have been reported to date. These assemblies have relied on the use of interactions that robustly direct 2D-assembly, such as large hydrophobic cores with strong π-stacking interactions,[62–64] peptide β-sheet formation,[65] or a precisely-designed DNA origami template ("frame-guided assembly").[66,67] The π-stacking core approach, in particular, resulted in the spontaneous formation of assemblies that were unaffected by DNA length and sequence. When the interactions were less strong, such as with "oligopyrenotides", only a maximum of one nucleotide could be included in the amphiphile structure to give nanosheets; the addition of further nucleotides shifted the morphology from 2D nanosheets to 1D nanoribbons.[68] To take advantage of the structural diversity of DNA amphiphiles as a macromolecular motif, there is a need for an improved understanding of their associated 2D self-assembly mechanisms, leading to systematic methods to create free-standing 2D sheets in water using these special block copolymers.[26,69,70]

Herein we report the supramolecular polymerization of sequence-defined triblock DNA amphiphiles into 2D nanosheets in aqueous solution. The modular structure of the DNA amphiphiles—comprising ssDNA, hexaethylene (C12) chains, and Cy3 dyes—and their sequence definition allow us to probe the mechanistic and morphological effect of subtle changes in amphiphile sequence and length on the supramolecular assembly. Our combined spectroscopic, imaging, and modeling study reveals the formation of a lipid bilayer-like structure akin to a cellular membrane as the most stable morphology. We report an unprecedented 2D assembly in which the terminal π-stacking chromophore block folds back and interacts with the hydrophilic DNA block on the surface of the nanosheets, leading to chiroptically active assemblies. We find that this intramolecular interaction is crucial to nanosheet formation and, interestingly, is dependent on the DNA sequence. This work provides mechanistic insights into the formation of supramolecular DNA structures resembling free-standing membrane bilayers, allowing us to visualize the parameter space of structural modifications and kinetic control critical to achieving the desired 2D morphology. Our results also raise the intriguing question of the potential role of other biologically active DNA binders in driving the assembly of 2D DNA amphiphile nanostructures.

Results and Discussion

Self-assembly of DNA nanosheets

The DNA amphiphiles **9a** (5′—$Cy3_2$-$C12_{12}$-TTT TTC AGT —3′) were generated on an automated DNA synthesizer as fully monodisperse, triblock structures, comprising: (i) a hydrophilic 9-mer DNA block, (ii) a hydrophobic block containing twelve linear hexaethylene (C12) chains and (iii) a π-stacking block containing two cyanine-3 (Cy3) chromophores (Figure 1a). The monomeric units in the structure are separated by negatively charged phosphate groups which confer water solubility. Room temperature (RT) aging a solution of these DNA amphiphiles in the presence of Mg^{2+} cations ($[Mg^{2+}]=12.5$ mM in 1x TAMg buffer) leads to the formation of nanofibers observed by atomic force microscopy (AFM) in air (Figure 1c). Subsequent annealing of the nanofibers—or direct annealing of a buffered DNA amphiphile solution without RT aging—yields rectangular, anisotropic nanosheets, observed by AFM in air (Figures 1b, d) and fluid (Figure 1e) as well as by transmission electron microscopy (TEM) (Figure 1f). The size of the nanosheets increases with cation and amphiphile concentration as observed by AFM (Figures SF14–15), native agarose gel electrophoresis (Figures SF118–119) and dynamic light scattering (DLS) (Figure SF120) suggesting that the cations serve to counterbalance the negative charges in the amphiphile structure and facilitate self-assembly. Cross-section analysis of the nanosheets using AFM reveals that the 2D structures have a uniform height of 10.0 ± 0.2 nm (Figure SF24). Replacing the Mg^{2+} cations with Na^+ ($[Na^+]=161.1$ mM) did not yield nanosheets or nanofibers (Figures SF16–17) whereas using a divalent cation mix of Mg^{2+} and Ca^{2+} at extracellular concentrations ($[Mg^{2+}]=1.5$ mM; $[Ca^{2+}]=2.5$ mM) yielded heterogeneous morphologies dependent on annealing conditions (Figures SF18–20).

Role of Cyanine-3 in morphology selection

The self-assembly of the DNA amphiphiles can be monitored using spectroscopic techniques, owing to the incorporation of Cy3 dyes in the amphiphile structure. Both the room temperature-aged fibers and annealed nanosheets show >80% decrease in fluorescence intensity relative to the free amphiphile in (the buffer-free control) solution (Figures SF141–142).[43] Consequently, we initially hypothesized that the hydrophobic Cy3 units may be buried and interacting together within the hydrophobic cores, resulting in aggregation-induced quenching. However, circular dichroism (CD) of **9a** nanosheets (Figure 2a(i), Figure SF121) showed clear CD signals in the Cy3 absorption region centered at 515 nm. Considering the achiral nature of the two hydrophobic blocks, this suggests that the Cy3 chromophore block might not be buried in the core but is possibly interacting with the chiral DNA component (Figure 2a(i)). Cyanine dyes are known to interact with DNA strands by end-stacking when placed at the strand termini, and by groove binding if placed within a strand.[71–73]

One advantage of our synthetic strategy is the ability to make sequence-defined polymers and change the composition one monomer at a time. To further elucidate the importance of Cy3 in the supramolecular polymerization process, we investigated the self-assembly of **9a-1** (Cy3-$C12_{12}$-TTT TTC AGT) and **9a-0** ($C12_{12}$-TTT TTC AGT), amphiphiles that differ from the primary sequence only in the number of Cy3 units appended to the 5′ end. Thermal annealing of these two amphiphiles leads to morphologically

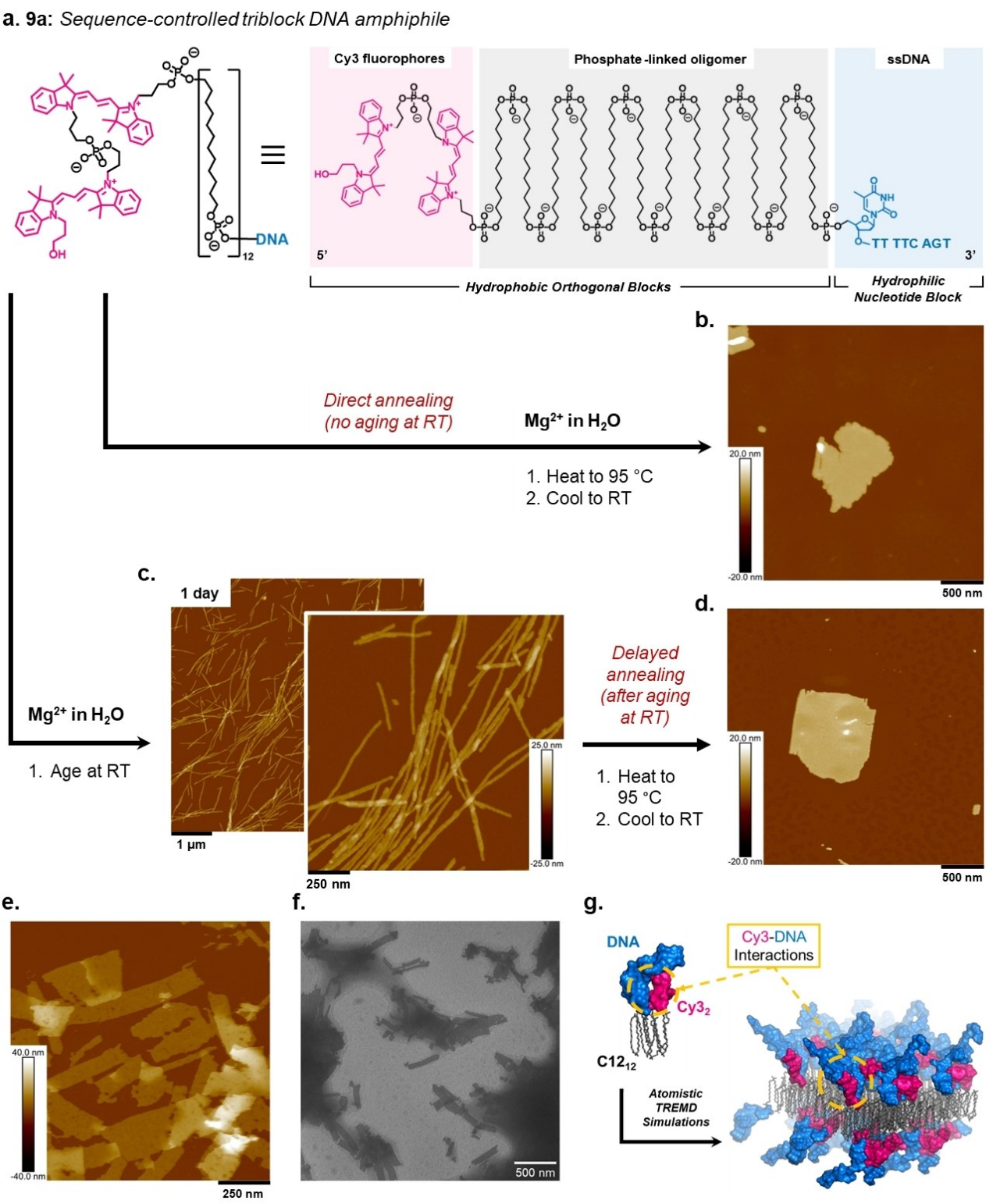

Figure 1. Supramolecular polymerization of lipid-like DNA amphiphiles. a) Triblock structure of the DNA amphiphile **9a** which undergoes self-assembly in Mg^{2+}-buffered aqueous solution to directly yield b) supramolecular 2D nanosheets or c) morphologically distinct 1D nanofibers when aged at room temperature that transform into d) 2D nanosheets upon annealing, as seen via AFM in air on mica. The nanosheet structures are also observed using e) AFM in fluid on mica and f) TEM. g) An atomistic model of the folded amphiphile and the nanosheet morphology simulated using temperature replica exchange molecular dynamics (TREMD) simulations. Height bars in nm.

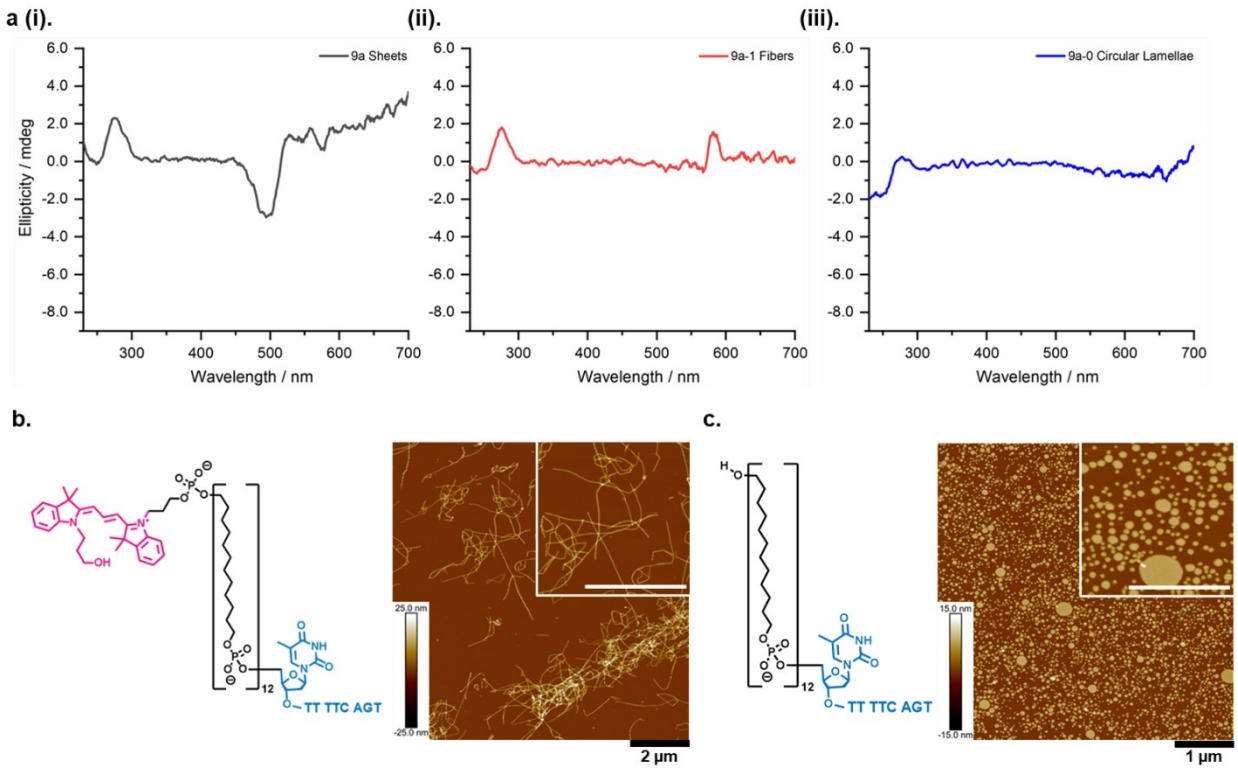

Figure 2. Role of Cy3 in determining supramolecular morphology: a) Comparison of the RT CD signals of i) **9a** nanosheets, (ii) **9a-1** nanofibers, and (iii) **9a-0** circular lamellae. AFM in air images show the formation of b) fibers from the annealing of **9a-1** and c) isotropic circular lamellae from the annealing of **9a-0**. Inset scale bars in white correspond to the same length as the black scale bars at the bottom of each image. Height bars in nm.

different structures: **9a-1** forms flexible fibers ($h = 9.0 \pm 0.5$ nm) instead of nanosheets (Figure 2b) whereas **9a-0** assembles into polydisperse, flat, circular structures ($h = 8.0 \pm 0.5$ nm) (Figure 2c). This suggests that the dye introduces anisotropy in the supramolecular structure as a result of π-stacking which leads to long-range order in the formation of the flexible fibers (**9a-1**) and nanosheets (**9a**) as opposed to isotropic circular lamellae (**9a-0**). The CD signal of **9a-0**, as expected, shows no Cy3-associated signals (Figure 2a(iii)) whereas that for **9a-1** (containing one Cy3) exhibits no distinct peak at *ca.* 500 nm (Figure 2a(ii)). This suggests that the 500 nm peak for **9a** (containing two Cy3 s, Figure 2a(i)) comes from *intra*molecular Cy3-Cy3 interactions in a dimer within the **9a** nanosheet assembly, arising from a chiral stacking of the dyes in proximity to the chiral DNA component.[74] Such an *intra*molecular interaction is not possible for **9a-1**. Thus, the Cy3 block plays a critical role in the morphology: self-assembly changes dramatically upon introducing a single Cy3 to **9a-0**, and a second Cy3 is needed for growth in the second dimension and formation of the nanosheet structure.

Reducing the number of C12 units in **9a** to 11 (**9a-HE11**) or 10 (**9a-HE10**) also results in anisotropic nanosheet formation (Figures SF94, 96) accompanied by the negative *ca.* 500 nm CD peak (Figures SF128a, 129a). For **9a-HE8** (containing eight C12 units), however, flat, nearly isotropic 2D assemblies ($h = 9.5 \pm 0.5$ nm) are observed upon annealing (Figure SF92) with a markedly strong CD response (Figure SF127a) that is discussed further below. These results suggest that at least some of the anisotropy in the nanosheet morphologies observed in our study is attributable to the number of C12 units in the amphiphiles. Replacing the Cy3 dyes in **9a** with two Cy5 dyes (**9a-Cy5**) results in the formation of flat, 2D assemblies ($h = 6.3 \pm 0.3$ nm) that are more uniform and square-shaped than the **9a** nanosheets (Figure SF114).

Molecular modeling of supramolecular nanosheets

The folding of the amphiphiles and their arrangement in the supramolecular assembly were explored using molecular modeling and simulation. We first investigated the architecture of the C12 chains by testing the intramolecular folding of **9a** amphiphiles using equilibrium and enhanced sampling molecular dynamics (MD) simulations (with Mg^{2+} ions present). We hypothesized that, due to its hydrophobicity, the most thermodynamically stable configurations of the $C12_{12}$ block would minimize its solvent-accessible surface area (SASA). Equilibrium MD simulations initiated from three different disordered initial configurations of the $C12_{12}$ block (Figure SF145) revealed large decreases in SASA over time. Unlike these disordered configurations, the hypothesized pre-folded, concertina-like **9a** ordered

structure[43] was found to remain stable and did not undergo C12 chain contraction (Figure SF145).

Next, temperature replica exchange molecular dynamics (TREMD) simulations were used to further interrogate the stability of this ordered structure at low (RT/27 °C) and high (annealing/97 °C) temperatures. The resulting converged SASA distributions demonstrated that the hypothesized compact structure was favored at low temperature but unfolded with mispacked C12 chains at elevated temperatures (Figure 3a). This result was further supported by the relative orientation of each pair of C12 chains ($C12_i$ and $C12_j$ in Figure 3a), which we used as an order parameter to characterize the folded or misfolded amphiphile structures (checkerboards in Figure 3a, bottom). Overall, our simulations support the formation of a stable, highly ordered, bilayer-type arrangement of the individual amphiphiles with the C12-connecting phosphate groups positioned at both solvent interfaces. Such an arrangement has previously been postulated for amphiphilic oligopyrenotides and azobenzene-based oligomers forming supramolecular 2D assemblies, based on experiments.[75–77]

After establishing the intramolecular folding of the amphiphiles, we tested the Mg^{2+}-dependent association of amphiphiles and constructed an atomistic model of the **9a** nanosheet morphology. Ordered amphiphiles were generated with sequential C12 chains aligned in a concertina arrangement, which placed the DNA and Cy3 dyes on one side of each amphiphile (Figure 3b). Entire amphiphiles were given alternating orientations to minimize steric clashing between the DNA and Cy3 blocks of adjacent folded amphiphiles when the C12 chains were placed in van der Waals contact. This leads to a checkerboard array of nine amphiphiles that were simulated using TREMD (Figure SF144) with periodic boundary conditions to mimic

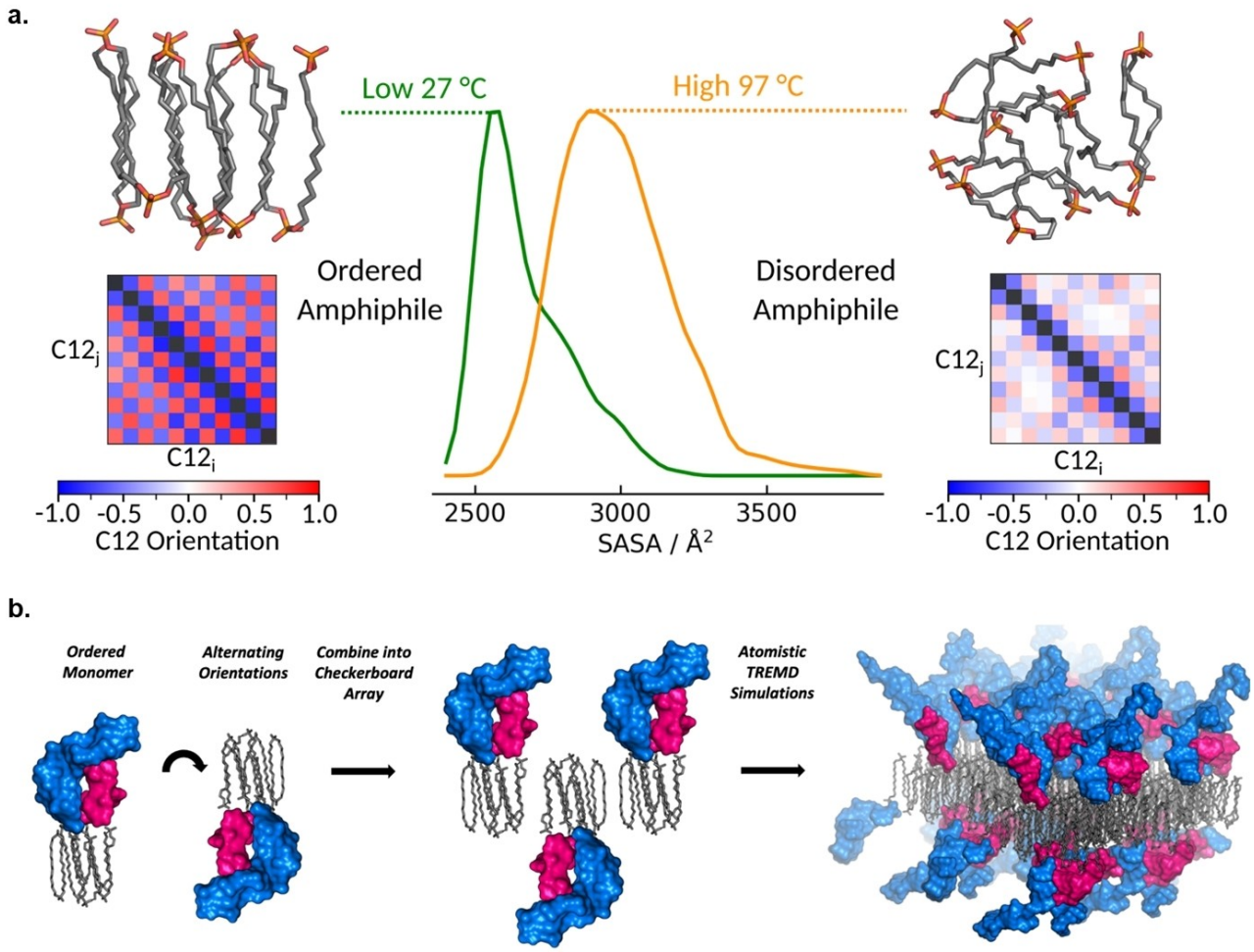

Figure 3. Folded and ordered amphiphiles as building blocks for 2D nanosheets. a) Distributions of the solvent accessible surface area (SASA) for the C12 chains of a **9a** amphiphile from low (27 °C) and high (97 °C) temperature rungs of temperature replica exchange molecular dynamics (TREMD) simulations (center). Example C12 structures from the SASA modes are shown for low (left) and high (right) temperature simulations and reveal differential degrees of C12 chain ordering (DNA and Cy3 hidden for clarity). Average C12 orientation order parameters from the last 25 ns of the TREMD simulations (lower left and right) further quantify the long-range chain ordering at low temperatures (left, e.g., C12 Orientation >0.5 for $i=1$ and $j=12$) and its disruption at high temperature (right). b) Alternating, checkerboard packing of nine **9a** amphiphiles followed by 3-μs TREMD simulations demonstrate a thermodynamically stable sheet structure (comprising nine amphiphiles). TREMD simulations were run at temperatures ranging from 27 to 97 °C. DNA block shown in blue, C12 chains in gray, and Cy3 dyes in magenta.

an infinite sheet. Like the ordered single amphiphile, at low temperatures the long-range order between C12 chains persisted throughout the simulations, supporting its stability for extended periods. Next, predictions about the Cy3-DNA interactions were made based on the MD simulations. We analyzed the mutual orientation preferences of the Cy3 indoles in the **9a** nanosheet at room temperature. Our data suggests that (i) the most populated orientation (Cy3-Cy3 angle: 60°, distance: 7.4 Å) occurs in close proximity to the DNA (Figure SF146a) and (ii) there is a strong preference of the Cy3 indoles to interact with the nucleobases proximal to the DNA–C12 interface and, to a much lesser extent, the terminal nucleobase at the 3′-end (Figure SF146b).

Using the same approach as for **9a**, atomistic models for **9a-1** and **9a-0** nanostructures (shown in Figure 2b, c) were simulated using TREMD and the thicknesses of the three amphiphile morphologies compared. The results supported the trends in height observed via AFM (Figure SF147). MD simulations of the nanosheet are thus consistent with a lipid bilayer-like arrangement of the C12 chains and folding back of the two Cy3 chromophores into close interaction with the DNA strand. This interaction is necessary for nanosheet formation and results in an induced CD peak for the Cy3 units *ca.* 500 nm. The $Cy3_2$-DNA interaction rigidifies the DNA strand at the interface between the DNA and hydrophobic units: this can result in decreasing the interfacial curvature and facilitating the two-dimensional growth of nanosheets. The stability of the **9a** nanosheets may also be explained in terms of Cy3 hydrophobic interactions rigidifying the folded amphiphile structure (Figure 3b); intramolecular interactions between end-modifications have been found to greatly enhance the stability of folded DNA structures.[78] These findings suggest that introducing other DNA-binding molecules into DNA amphiphiles—many of which are drugs[71]—may also profoundly affect the self-assembly and redirect the final morphology.

DNA sequence dependence

The Cy3-DNA interactions observed by CD spectroscopy and modeled by our MD simulations raise the important question of the sensitivity of the supramolecular polymerization process to DNA sequence. To investigate this, we synthesized a DNA amphiphile, **9b** ($Cy3_2$-$C12_{12}$-ATT CTA CTT), comprising a random nucleotide sequence different from the one in **9a** and tested it for self-assembly. Similar to the primary amphiphile (**9a**), **9b** assembles into nanosheets (Figure 4a(i)) 10.0 ± 0.3 nm thick upon thermal annealing and likewise displays the characteristic negative CD peak *ca.* 500 nm (Figure 4a(ii)).

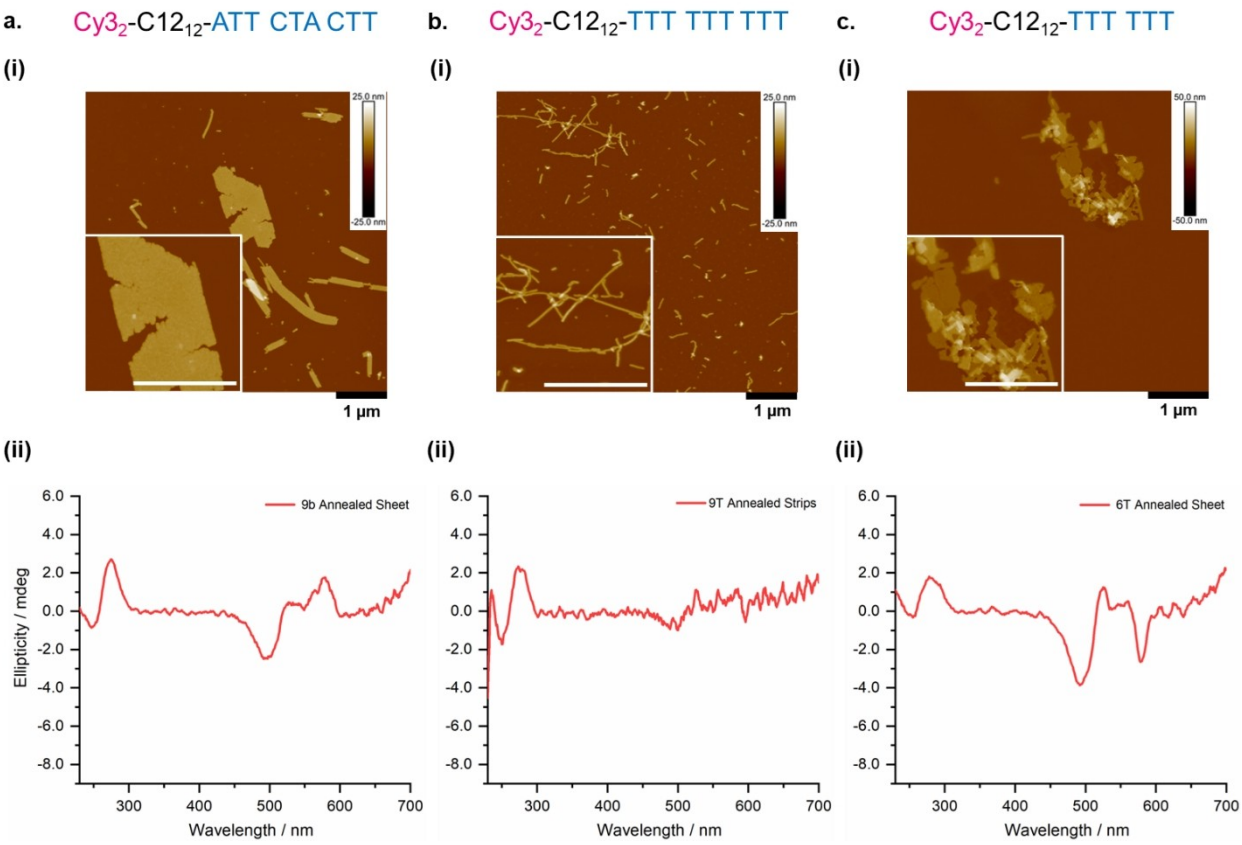

Figure 4. Role of DNA sequence in determining morphology: i) AFM in air images showing the nanostructures formed following annealing and (ii) the corresponding CD spectra for a) **9b** b) **9T** and c) **6T**. Inset scale bars in white correspond to the same length as the black scale bars at the bottom of each image. Height bars in nm.

We next explored the self-assembly of a DNA amphiphile with a poly-thymine (poly-T) 9-mer oligonucleotide sequence as the hydrophilic block: **9T** ($Cy3_2$-$C12_{12}$-T_9). Annealing the amphiphile solution of **9T** leads to flat, strip-like assemblies ($h \approx 9.5$ nm) that display a very limited propensity to stack laterally to form nanosheets (Figure 4b(i)). Intriguingly as well, the CD spectrum for these structures lacks the distinguishing features observed for the morphologies associated with the other amphiphiles discussed thus far (Figure 4b(ii)). This, coupled with the absence of any signals (apart from the DNA signal at 260 nm) in the CD spectrum, suggests that the poly-T oligonucleotide sequence in **9T** appears to disrupt the Cy3-DNA interactions that are essential to nanosheet formation and that result in the intramolecular Cy3-Cy3 excitonic coupling CD peak.

We hypothesize that these startling results are due to the flexibility of poly-T ssDNA compared to an arbitrary ssDNA sequence.[79] The greater conformational mobility of the ssDNA block in **9T** compared to **9a** and **9b** may result both in greater interfacial curvature of the assembly as well as a different interaction of the ssDNA block with the Cy3 dyes during the self-assembly process. The latter could disrupt *intra*molecular dye-dye interactions, as suggested by the lack of clear CD signals. A previous study has demonstrated that a poly-T 20-mer ssDNA is flexible enough to conformationally adopt a hairpin-like structure to preferentially bind a Gel Red bis-intercalating dye, unlike other ssDNA homo-oligonucleotides.[79] It is noteworthy that the **9T** sequence differs from **9a** and **9b** only in three and four nucleotides, respectively (see Table ST1). However, given the short (nine-nucleotide) length of the DNA blocks in the three amphiphiles, this translates into a significant difference.

We further explored this DNA sequence dependence of the supramolecular morphology using MD simulations. Radius of gyration measurements show that the mixed DNA sequence in **9a** undergoes unfolding as temperature is increased with the formation of larger extended structures (Figure SF148). In contrast, **9T** does not form compact structures at low temperature and is far more disordered at low and high temperatures—**9T** is thus more flexible and extended in comparison to **9a**.

We reasoned that shortening the DNA block in the amphiphile would reduce the flexibility of the poly-T sequence—thereby decreasing the interfacial curvature and increasing the packing parameter, leading to sheet formation. We thus synthesized and tested **6T** ($Cy3_2$-$C12_{12}$-T_6), an amphiphile with a six-nucleotide poly-T DNA block which, upon annealing, yielded the predicted 2D nanosheet morphology (Figure 4c(i)). The nanosheet structure now exhibited the characteristic negative CD peak *ca.* 500 nm (Figure 4c(ii)), suggesting a reinstatement of *intra*molecular dye-dye interactions. MD simulations also showed that, like **9a**, **6T** forms lower radius of gyration structures due to its truncated length, exhibiting limited flexibility (Figure SF148). These observations point to the interplay of two parameters in defining the assembly of DNA nanosheets: the interaction of the $Cy3_2$ chromophore block with DNA, and the role of DNA sequence—flexible, polyT sequences prevent nanosheet formation, while more rigid, mixed DNA sequences result in 2D-growth into nanosheets.

Supramolecular polymerization mechanism and pathway complexity

As discussed above, the annealing method is crucial to the formation of the 2D nanosheet structure. Aging an aqueous solution of **9a** at room temperature leads to the formation of nanofibers instead of nanosheets ($[Mg^{2+}] = 12.5$ mM in 1× TAMg buffer, Figure 1c); this starts to occur within minutes of buffer addition to the solution. AFM images from early time points (15 mins, 30 mins) reveal the presence of spherical and very short cylindrical micellar structures in addition to the fibers (Figures SF46, 48). This observation, in addition to the segmented appearance of the fibers at these earlier time points, suggests that fiber formation is a possible structural evolution arising from the 1D end-to-end assembly of short micelles or cylinders. This is further discussed in the Supporting Information (Section 6).

To further study the polymorphism observed in the supramolecular polymerization of **9a**, the room temperature-aged fibers were slowly heated to 95 °C and then slowly cooled back to room temperature, and the process was monitored by AFM sampling every 10 °C (heating/cooling rate 0.1 °C/s, Figure 5a, Figures SF61–68). During the heating stage, at lower temperatures along the thermal gradient (35 °C), the fibers retain their 1D morphology (Figure 5a, Figure SF61). As the temperature is increased, the morphology gives way to 1D ribbons (65–75 °C) with segmented tapeworm-like structures that are flatter and broader at higher temperatures (75 °C) (Figure 5a, Figure SF63). A structural collapse is observed at 85 °C yielding flexible fibers and toroidal structures. The toroids are likely a closed loop version of the amorphous fibers. This interesting morphology may arise from possible "softening" of the hydrophobic core at higher temperature followed by curvature, to minimize exposure of the fiber ends to the aqueous solution; this mechanism, however, will require further investigation. During the cooling stage, sheets form slowly at 65 °C, with larger populations as the system approaches room temperature. The nanosheets obtained from heating the fibers appear to be similar to the ones obtained by directly annealing the amphiphiles in buffer solution (Figures SF30–45). Our observations thus suggest a competitive self-assembly mechanism, wherein off-pathway, kinetically trapped fiber structures vie against thermodynamically favored on-pathway nanosheet assemblies, and can be converted to these nanosheets upon heating and then cooling. The fiber assemblies of **9a** (and **9b**) are disrupted upon addition of complemetary ssDNA sequences (**9a′** and **9b′**) at room temperature (Figures SF109, 111) unlike the nanosheets which are formed upon annealing despite the addition of the complementary strands (Figures SF110, 112); this behavior emphasizes the thermodynamic stability of the nanosheets.

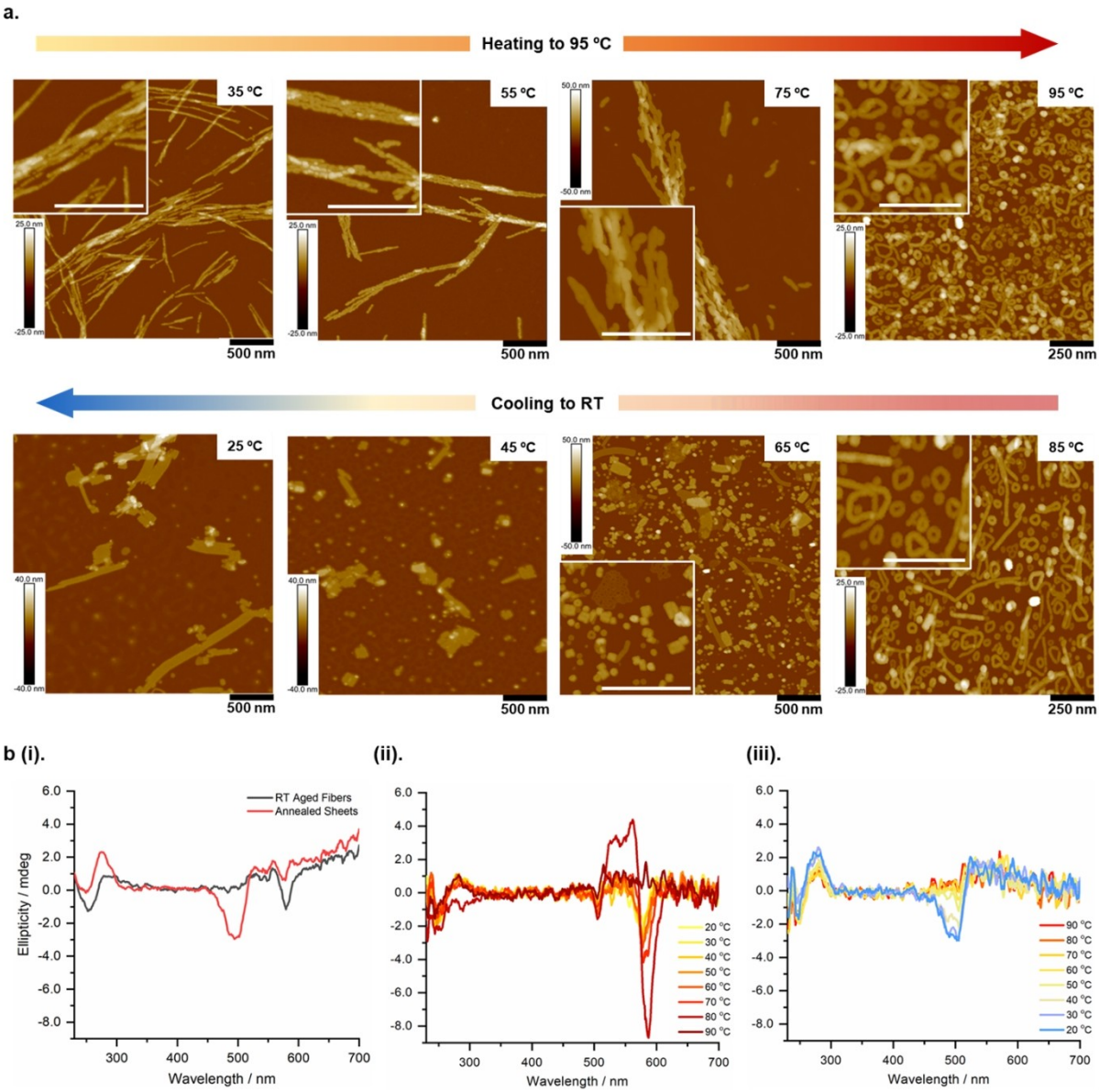

Figure 5. Temperature-dependent AFM and CD reveal a complex pathway with morphological diversity. a) Heating results in the flattening of the fibers into 1D ribbons followed by a thermal collapse into flexible fibers that fold into toroidal "donuts", as seen in AFM in air images. Cooling the system to room temperature results in the formation of sheets from the flexible fibers present at higher temperatures. b) The corresponding morphological changes can also be tracked via variable temperature CD data which is indicative of Cy3 packing in the fibers and sheets i) at room temperature and during the annealing cycle while (ii) heating and (iii) cooling. Inset scale bars in white correspond to the same length as the black scale bars at the bottom of each image. Height bars in nm.

The CD spectrum for the nanofibers of **9a** shows a distinct negative CD peak *ca.* 580 nm suggesting differences in Cy3 packing and interaction compared to the nanosheets (Figure 5b (i)). Variable temperature CD spectroscopy reveals further clues regarding the thermal rearrangement of the Cy3 dyes during the (nanofiber→nanosheet) morphological transformation (Figure 5b (ii), (iii)). Increasing the temperature leads to the nanofiber signal becoming significantly more pronounced, resolving into observable bisignate curves (centered at 565 and 515 nm) at 80 °C, just before the onset of structural collapse. These signals disappear at 90 °C indicating an absence of Cy3 chirality in the flexible fibers and toroidal structures present at this temperature. No Cy3 CD signal was observed upon thermal annealing of the buffer and salt-free control solution of **9a**; the amphiphile is incapable of assembling in these conditions and remains monomeric (Figure SF125a). This suggests that the pronounced CD signals at 80 °C arise due to excitonic coupling between Cy3 dyes within the nanostructure. Intriguingly, the CD spectra for both the aged and annealed **9a-HE8** samples show the same distinct bisignate signals when measured at room temperature, as those for **9a** (containing HE12) at 80 °C. (Figure SF127a). This result suggests that reducing the number of C12 units to eight facilitates increased dye-

dye interactions and leads to a pronounced increase in chirality for the Cy3 dyes, possibly due to the increased flexibility of the core with shorter hydrophobic chains.

Additional support for this analysis comes from a recent study, which evaluated Cy3-Cy3 dimer interactions within a DNA DX tile.[80] The physical positioning of adjacent, covalently-linked Cy3 dyes within the DX scaffold was found to result in strong electronic coupling between the dyes, and was marked by the bisignate CD signal centered at 565 nm—similar to what is observed at 80 °C during the heating stage for **9a** (and at ambient conditions for **9a-HE8**). Likewise, a distinctive negative CD peak *ca.* 500 nm —similar to that for our nanosheets at room temperature— was observed for DX tile configurations with distorted arrangements of the Cy3 dimers within the scaffold.[80] Taken collectively, this suggests that the room temperature, off-pathway nanofiber morphology in our studies involves weak Cy3-Cy3 interactions; heating the system (or reducing the number of C12 units to eight) results in thermal (or physical) rearrangement of the dyes leading to strong excitonic coupling, which gives way to a distorted configuration in the nanosheets upon cooling to room temperature. The most populated Cy3-Cy3 orientation observed from the molecular dynamics results (see above, Figure SF146a) may be one such distorted configuration.

Conclusion

Elucidating the self-assembly pathways of water-soluble block copolymers such as DNA amphiphiles is critical for their use as macromolecular motifs for 2D supramolecular assemblies in aqueous systems. Unlike most conventionally synthesized BCPs, the self-assembly mechanism and subsequent morphology for DNA amphiphiles were found to be sensitive to: (i) folding back of a DNA-binding molecule block and its interactions with DNA and (ii) subtle changes in the DNA sequence. Thermally-induced chain folding within the C12 block was crucial for the formation of a compact, lipid-like bilayer arrangement within the core, while the Cy3 block with two dyes was necessary for the introduction of long-range two-dimensional order and formation of the nanosheet structure. The behavior of the Cy3 block, in turn, was influenced by its interactions with the ssDNA, which were sensitive to DNA sequence and length. By systematically modifying these parameters, we were able to evaluate their effect on both the supramolecular polymerization mechanism and morphology. Our work sheds light on the structural and mechanistic controls that can be employed to achieve supramolecular polymerization of free-standing 2D nanosheets in water using DNA amphiphiles. In particular, it emphasizes that the DNA sequence is an important structural parameter dictating orthogonal intramolecular interactions beyond the Watson–Crick-Franklin base-pairing regime. This study also highlights the potential for the exploitation of biologically active DNA binders and dyes within amphiphile structures to create functional 2D nanosheets via block copolymer assembly.

Acknowledgements

This work was funded by the Natural Science and Engineering Research Council of Canada (NSERC), Canada Foundation for Innovation (CFI), and Fonds de Recherche du Québec—Nature et Technologies (FRQNT). M. G. R. thanks the NSERC for a Vanier Scholarship and the FRQNT for a Doctoral Research Scholarship (B2Z). H. F. S. is thankful to Canada Research Chairs Program, Canada Council for the Arts for a Killam Fellowship; H. F. S. is a Cottrell Scholar of the Research Corporation. J. M. R. and J. L. were partially supported by an NIH R01 award (R01GM129431 to J. L.) and F. C. was supported by an NSF award (CHE-1945394 to J. L.).

Conflict of Interest

The authors declare no conflict of interest.

Data Availability Statement

The data that support the findings of this study are available from the corresponding author upon reasonable request.

Keywords: DNA · Molecular Dynamics Simulations · Nanosheets · Self-Assembly · Sequence-Controlled Polymers

[1] N. R. Council, *Hierarchical Structures in Biology as a Guide for New Materials Technology*, National Academies Press, Washington, D. C., **1994**, p. 17.
[2] B. Alberts, A. Johnson, J. Lewis, M. Raff, K. Roberts, P. Walter, *Molecular Biology of the Cell*, Garland Science, New York, **2002**, p. 565.
[3] Y. Mai, A. Eisenberg, *Chem. Soc. Rev.* **2012**, *41*, 5969.
[4] B. Lotz, A. J. Kovacs, G. A. Bassett, A. Keller, *Kolloid Z. Z. Polym.* **1966**, *209*, 115–128.
[5] J. Wang, W. Zhu, B. Peng, Y. Chen, *Polymer* **2013**, *54*, 6760–6767.
[6] S.-C. Chan, S.-W. Kuo, C.-H. Lu, H.-F. Lee, F.-C. Chang, *Polymer* **2007**, *48*, 5059–5068.
[7] M. Su, H. Huang, X. Ma, Q. Wang, Z. Su, *Macromol. Rapid Commun.* **2013**, *34*, 1067–1071.
[8] H. Qiu, Y. Gao, C. E. Boott, O. E. C. Gould, R. L. Harniman, M. J. Miles, S. E. D. Webb, M. A. Winnik, I. Manners, *Science* **2016**, *352*, 697–701.
[9] Z. M. Hudson, C. E. Boott, M. E. Robinson, P. A. Rupar, M. A. Winnik, I. Manners, *Nat. Chem.* **2014**, *6*, 893–898.
[10] X. He, Y. He, M.-S. Hsiao, R. L. Harniman, S. Pearce, M. A. Winnik, I. Manners, *J. Am. Chem. Soc.* **2017**, *139*, 9221–9228.
[11] Y. Mai, A. Eisenberg, *Chem. Soc. Rev.* **2012**, *41*, 5969–5985.
[12] Z. Li, Y. Zhang, L. Wu, W. Yu, T. R. Wilks, A. P. Dove, H. M. Ding, R. K. O'Reilly, G. Chen, M. Jiang, *ACS Macro Lett.* **2019**, *8*, 596–602.
[13] G. Rizis, T. G. M. van de Ven, A. Eisenberg, *Angew. Chem. Int. Ed.* **2014**, *53*, 9000–9003.
[14] Z. X. Du, J. T. Xu, Z. Q. Fan, *Macromolecules* **2007**, *40*, 7633–7637.
[15] S. Ganda, M. Dulle, M. Drechsler, B. Förster, S. Förster, M. H. Stenzel, *Macromolecules* **2017**, *50*, 8544–8553.

[16] B. Dai, D. Li, W. Xi, F. Luo, X. Zhang, M. Zou, M. Cao, J. Hu, W. Wang, G. Wei, Y. Zhang, C. Liua, *Proc. Natl. Acad. Sci. USA* **2015**, *112*, 2996–3001.

[17] J. Sun, R. N. Zuckermann, *ACS Nano* **2013**, *7*, 4715–4732.

[18] F. Jiao, Y. Chen, H. Jin, P. He, C. L. Chen, J. J. De Yoreo, *Adv. Funct. Mater.* **2016**, *26*, 8960–8967.

[19] H. Jin, F. Jiao, M. D. Daily, Y. Chen, F. Yan, Y.-H. Ding, X. Zhang, E. J. Robertson, M. D. Baer, C.-L. Chen, *Nat. Commun.* **2016**, *7*, 12252.

[20] K. T. Nam, S. A. Shelby, P. H. Choi, A. B. Marciel, R. Chen, L. Tan, T. K. Chu, R. A. Mesch, B. C. Lee, M. D. Connolly, C. Kisielowski, R. N. Zuckermann, *Nat. Mater.* **2010**, *9*, 454–460.

[21] J. Ma, B. Cai, S. Zhang, T. Jian, J. J. de Yoreo, C. L. Chen, F. Baneyx, *Nano Lett.* **2021**, *21*, 1636–1642.

[22] E. J. Robertson, G. K. Olivier, M. Qian, C. Proulx, R. N. Zuckermann, G. L. Richmond, *Proc. Natl. Acad. Sci. USA* **2014**, *111*, 13284–13289.

[23] B. Sanii, R. Kudirka, A. Cho, N. Venkateswaran, G. K. Olivier, A. M. Olson, H. Tran, R. M. Harada, L. Tan, R. N. Zuckermann, *J. Am. Chem. Soc.* **2011**, *133*, 20808–20815.

[24] R. Kudirka, H. Tran, B. Sanii, K. T. Nam, P. H. Choi, N. Venkateswaran, R. Chen, S. Whitelam, R. N. Zuckermann, *Biopolymers* **2011**, *96*, 586–595.

[25] E. J. Robertson, C. Proulx, J. K. Su, R. L. Garcia, S. Yoo, E. M. Nehls, M. D. Connolly, L. Taravati, R. N. Zuckermann, *Langmuir* **2016**, *32*, 11946–11957.

[26] P. Mu, G. Zhou, C. L. Chen, *Nano-Struct. Nano-Objects* **2018**, *15*, 153–166.

[27] M. Vybornyi, Y. Vyborna, R. Häner, *Chem. Soc. Rev.* **2019**, *48*, 4347–4360.

[28] S. K. Albert, M. Golla, N. Krishnan, D. Perumal, R. Varghese, *Acc. Chem. Res.* **2020**, *53*, 2668–2679.

[29] T. Schnitzler, A. Herrmann, *Acc. Chem. Res.* **2012**, *45*, 1419–1430.

[30] M. Kwak, A. Herrmann, *Chem. Soc. Rev.* **2011**, *40*, 5745–5755.

[31] Y. Wu, K. Sefah, H. Liu, R. Wang, W. Tan, *Proc. Natl. Acad. Sci. USA* **2010**, *107*, 5–10.

[32] T. G. W. Edwardson, K. M. M. Carneiro, C. J. Serpell, H. F. Sleiman, *Angew. Chem. Int. Ed.* **2014**, *53*, 4567–4571.

[33] J. H. Jeong, T. G. Park, *Bioconjugate Chem.* **2001**, *12*, 917–923.

[34] Z. Li, Y. Zhang, P. Fullhart, C. A. Mirkin, *Nano Lett.* **2004**, *4*, 1055–1058.

[35] R. J. Banga, B. Meckes, S. P. Narayan, A. J. Sprangers, S. T. Nguyen, C. A. Mirkin, *J. Am. Chem. Soc.* **2017**, *139*, 4278–4281.

[36] F. E. Alemdaroglu, K. Ding, R. Berger, A. Herrmann, *Angew. Chem. Int. Ed.* **2006**, *45*, 4206–4210.

[37] C. J. Kim, X. Hu, S. J. Park, *J. Am. Chem. Soc.* **2016**, *138*, 14941–14947.

[38] S. K. Albert, H. V. P. Thelu, M. Golla, N. Krishnan, S. Chaudhary, R. Varghese, *Angew. Chem. Int. Ed.* **2014**, *53*, 8352–8357.

[39] S. K. Albert, H. V. P. Thelu, M. Golla, N. Krishnan, R. Varghese, *Nanoscale* **2017**, *9*, 5425–5432.

[40] S. K. Albert, M. Golla, H. V. P. Thelu, N. Krishnan, R. Varghese, *Chem. Eur. J.* **2017**, *23*, 8348–8352.

[41] C. D. Bösch, J. Jevric, N. Bürki, M. Probst, S. M. Langenegger, R. Häner, *Bioconjugate Chem.* **2018**, *29*, 1505–1509.

[42] S. Rothenbühler, I. Iacovache, S. M. Langenegger, B. Zuber, R. Häner, *Nanoscale* **2020**, *12*, 21118–21123.

[43] D. Bousmail, P. Chidchob, H. F. Sleiman, *J. Am. Chem. Soc.* **2018**, *140*, 9518–9530.

[44] S. P. W. Wijnands, W. Engelen, R. P. M. Lafleur, E. W. Meijer, M. Merkx, *Nat. Commun.* **2018**, *9*, 65.

[45] L. Wang, Y. Feng, Z. Yang, Y. M. He, Q. H. Fan, D. Liu, *Chem. Commun.* **2012**, *48*, 3715–3717.

[46] K. M. M. Carneiro, N. Avakyan, H. F. Sleiman, *Wiley Interdiscip. Rev. Nanomed. Nanobiotechnol.* **2013**, *5*, 266–285.

[47] M. Golla, S. K. Albert, S. Atchimnaidu, D. Perumal, N. Krishnan, R. Varghese, *Angew. Chem. Int. Ed.* **2019**, *58*, 3865–3869.

[48] Y. Vyborna, M. Vybornyi, A. V. Rudnev, R. Häner, *Angew. Chem. Int. Ed.* **2015**, *54*, 7934–7938.

[49] Y. Vyborna, M. Vybornyi, R. Häner, *J. Am. Chem. Soc.* **2015**, *137*, 14051–14054.

[50] Y. Vyborna, M. Vybornyi, R. Häner, *Chem. Commun.* **2017**, *53*, 5179–5181.

[51] J. J. Fakhoury, T. G. Edwardson, J. W. Conway, T. Trinh, F. Khan, M. Barłóg, H. S. Bazzi, H. F. Sleiman, *Nanoscale* **2015**, *7*, 20625–20634.

[52] A. M. Rush, M. P. Thompson, E. T. Tatro, N. C. Gianneschi, *ACS Nano* **2013**, *7*, 1379–1387.

[53] D. Bousmail, L. Amrein, J. J. Fakhoury, H. H. Fakih, J. C. C. Hsu, L. Panasci, H. F. Sleiman, *Chem. Sci.* **2017**, *8*, 6218–6229.

[54] H. H. Fakih, J. J. Fakhoury, D. Bousmail, H. F. Sleiman, *ACS Appl. Mater. Interfaces* **2019**, *11*, 13912–13920.

[55] Y. Wu, K. Sefah, H. Liu, R. Wang, W. Tan, *Proc. Natl. Acad. Sci. USA* **2010**, *107*, 5–10.

[56] A. L. Prinzen, D. Saliba, C. Hennecker, T. Trinh, A. Mittermaier, H. F. Sleiman, *Angew. Chem. Int. Ed.* **2020**, *59*, 12900–12908.

[57] M. D. Dore, J. J. Fakhoury, A. Lacroix, H. F. Sleiman, *Chem. Commun.* **2018**, *54*, 11296–11299.

[58] T. Trinh, P. Chidchob, H. S. Bazzi, H. F. Sleiman, *Chem. Commun.* **2016**, *52*, 10914–10917.

[59] T. Zhang, C. H. Zhang, *J. Mater. Chem. B* **2019**, *7*, 7736–7743.

[60] Y. Kim, X. Liu, H. Li, M. Lee, *Chem. Asian J.* **2019**, *14*, 952–957.

[61] N. Krishnan, D. Perumal, S. Atchimnaidu, K. S. Harikrishnan, M. Golla, N. M. Kumar, J. Kalathil, J. Krishna, D. K. Vijayan, R. Varghese, *Chem. Eur. J.* **2020**, *26*, 1037–1041.

[62] S. K. Albert, I. Sivakumar, M. Golla, H. V. P. Thelu, N. Krishnan, K. L. Joseph Libin, Ashish, R. Varghese, *J. Am. Chem. Soc.* **2017**, *139*, 17799–17802.

[63] N. Krishnan, M. Golla, H. V. P. Thelu, S. K. Albert, S. Atchimnaidu, D. Perumal, R. Varghese, *Nanoscale* **2018**, *10*, 17174–17181.

[64] C. J. Kim, J. eun Park, X. Hu, S. K. Albert, S. J. Park, *ACS Nano* **2020**, *14*, 2276–2284.

[65] S. K. Albert, S. Lee, P. Durai, X. Hu, B. Jeong, K. Park, S. Park, *Small* **2021**, *17*, 2006110.

[66] C. Zhou, Y. Zhang, Y. Dong, F. Wu, D. Wang, L. Xin, D. Liu, *Adv. Mater.* **2016**, *28*, 9819–9823.

[67] Y. Dong, Y. Yang, C. Lin, D. Liu, *Acc. Chem. Res.* **2022**, *55*, 1938–1948.

[68] Y. Vyborna, S. Altunbas, M. Vybornyi, R. Häner, *Chem. Commun.* **2017**, *53*, 12128–12131.

[69] X. Ma, S. Zhang, F. Jiao, C. J. Newcomb, Y. Zhang, A. Prakash, Z. Liao, M. D. Baer, C. J. Mundy, J. Pfaendtner, A. Noy, C. L. Chen, J. J. De Yoreo, *Nat. Mater.* **2017**, *16*, 767–774.

[70] B. Sanii, T. K. Haxton, G. K. Olivier, A. Cho, B. Barton, C. Proulx, S. Whitelam, R. N. Zuckermann, *ACS Nano* **2014**, *8*, 11674–11684.

[71] M. J. Morten, S. G. Lopez, I. Emilie Steinmark, A. Rafferty, S. W. Magennis, *Nucleic Acids Res.* **2018**, *46*, 11618–11626.

[72] D. Heussman, J. Kittell, P. H. von Hippel, A. H. Marcus, *J. Chem. Phys.* **2022**, *156*, 045101.

[73] B. A. Armitage, in *DNA Binders and Related Subjects. Topics in Current Chemistry, Vol. 253* (Eds.: M. J. Waring, J. B. Chaires), Springer, Berlin, Heidelberg, **2005**, pp. 55–76.

[74] F. Nicoli, M. K. Roos, E. A. Hemmig, M. Di Antonio, R. de Vivie-Riedle, T. Liedl, *J. Phys. Chem. A* **2016**, *120*, 9941–9947.

[75] O. Vybornyi, S.-X. Liu, R. Häner, *Angew. Chem. Int. Ed.* **2021**, *60*, 25872–25877.

[76] M. Vybornyi, A. V. Rudnev, S. M. Langenegger, T. Wandlowski, G. Calzaferri, R. Häner, *Angew. Chem. Int. Ed.* **2013**, *52*, 11488–11493.
[77] M. Vybornyi, A. Rudnev, R. Häner, *Chem. Mater.* **2015**, *27*, 1426–1431.
[78] Y. Sun, H. Liu, L. Xu, L. Wang, Q.-H. Fan, D. Liu, *Langmuir* **2010**, *26*, 12496–12499.
[79] R. J. Sapia, C. Campbell, A. J. Reed, V. B. Tsvetkov, Y. V. Gerasimova, *Dyes Pigm.* **2021**, *188*, 109209.
[80] S. M. Hart, X. Wang, J. Guo, M. Bathe, G. S. Schlau-Cohen, *J. Phys. Chem. Lett.* **2022**, *13*, 1863–1871.

Manuscript received: December 5, 2022
Accepted manuscript online: March 20, 2023
Version of record online: May 8, 2023